Effect of Model Complexity on Fiber Activation Estimates in a Wearable Neuromodulator for Migraine

Enver Salkim, Arsam Shiraz, and Andreas Demosthenous
Electronic and Electrical Department, University College London, Torrington Place, WC1E 7JE, London, UK.
{E-mail: enver.salkim.14; a. shiraz; a.demosthenous@ucl.ac.uk}

***Abstract*—Migraine is a prevalent and highly disabling disorder. The pharmaceutical and invasive treatment methods have trouble-some side effects and associated risks, hence undesirable. Transcutaneous supraorbital neuromodulation has been shown to potentially suppress episodic migraine attacks yet results have low efficacy. This inconclusive response may be associated with neuroanatomical variations of patients which may be investigated using computational models. Model complexity is a limiting factor in implementing such techniques. This paper investigates the effect of model complexity on fiber activation estimates in transcutaneous frontal nerve stimulation. It is shown that the model can be simplified while minimally affecting the outcome.**

Keywords— Computational models, frontal nerve, migraine, neuromodulation.

I. INTRODUCTION

Migraine is classified as a primary headache with associated symptoms of throbbing headache, nausea and/or vomiting, photophobia (sensitivity to light) and phonophobia (sensitivity to sound). Its worldwide prevalence is around 15% of the population and women are affected more than men [1]. It has been identified as the seventh major disabling condition [2]. During migraine attacks, 75% of patients cannot function and nearly half of them need help from others [3]. In addition to direct healthcare costs, an indirect impact on the economy is that patients cannot continue to work which results in losses in the region of 20 million working days a year [1].

In general, migraine solutions are categorized as pharmaceutical and those based on neuromodulation techniques. The pharmaceutical methods have intolerable side-effects and limited efficacy (on average they reduce migraine attacks by about 50% in approximately 40–45% of patients) and[4]. Neuromodulation techniques may be subdivided to cutaneous (invasive) electrical nerve stimulation and transcutaneous (non-invasive) electrical nerve stimulation (TENS). The former require surgery, which is risky; they would be used only for chronic patients who have failed to respond to available non-invasive and pharmaceutical therapies [5]. Although some non-invasive neuromodulation techniques have provided positive results, most of them have had small numbers of participants and lacked control studies [6], [7].

The trigeminal nerve has a crucial role in headaches [8]. The supraorbital nerve (SON) and supratrochlear nerve (STN) arise from the frontal branch of the ophthalmic division of the trigeminal nerve. Transcutaneous supraorbital nerve stimulation (t-SNS) with Cefaly (Cefaly, CEFALY Technology, Liège, Belgium) stimulator has been developed to prevent episodic migraine by stimulating the SON and STN. Existing literature [6], [7] suggest the t-SNS with Cefaly device has more objective results as it includes large scale studies compared with other neuromodulation techniques aiming to prevent episodic migraine. However, there is some uncertainty about the efficacy of the device in migraine prevention. This limitation may be due to anatomical variations between individuals [9]. Hybrid computational models may be used to estimate current thresholds in neuromodulation therapy [10], [11] and investigate the effects of various parameters. However, when the computational complexity increases, the time and computational resources may limit the investigations. Therefore, to reduce the complexity and save computation time, the human head model may be built from simplified geometries that only describe the region of interest with a level of error. In this paper the results from a highly detailed human head model based on magnetic resonance imaging (MRI) studies and those of a simplified head model are compared to assess the usability of simplified models in future investigations.

The rest of the paper is organized as follows. Section II details the methods to generate the multilayer head volume conductor and nerve cable model and the subsequent investigations. The percentage activation estimates and current density of nerve fibers are reported in Section III. Discussion and conclusions outlining future directions are presented in Sections IV and V respectively.

For all the subsequent simulations and operations, a computer with an Intel Core i7-6700 CPU @ 3.4 GHz with 64 GB RAM was used.

II. METHODS

A. Realistic Human Head Model Development

A realistic three dimensional (3D) volume conductor model of human head was derived from MRI scans of the head of a healthy adult male subject [12]. Different head tissue layers such as skin (stratum corneum, epidermis, and dermis), fat, muscle, eyeball, skull, cerebrospinal fluid (CSF), and the brain (gray and white matter) were segmented based on high resolution MRI data using both automatic and manual segmentation processes in Simpleware ScanIP v2016.09

This work was funded by a PhD scholarship to E. Salkim by the Turkish Government, Ministry of National Education, and Mus Alpaslan University.

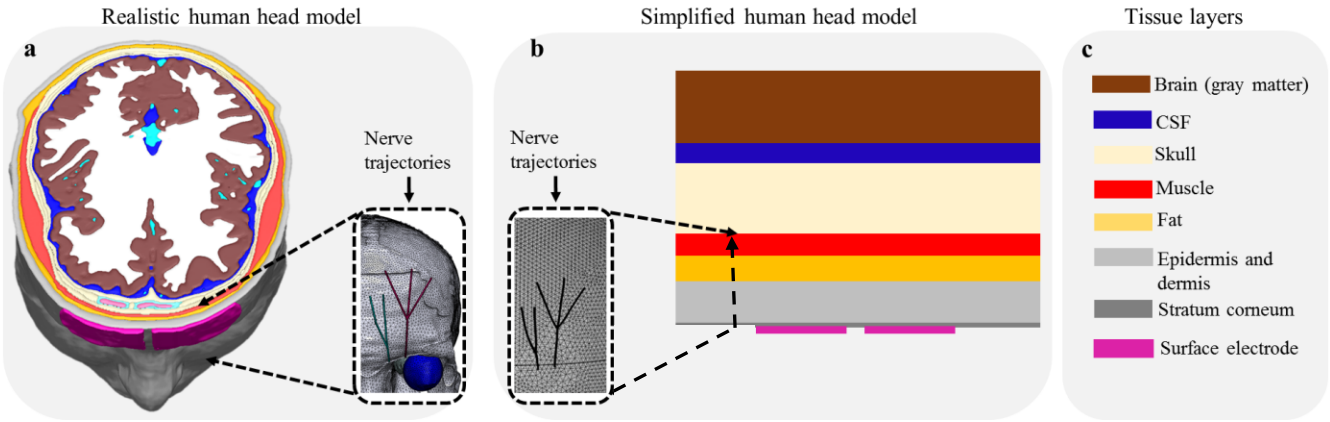

Fig. 1. A realistic (a) and a simplified human head model (b) and relative tissue layers (c) are shown. Each of tissue layers were represented with the same color for the two head models. However, the small structures such as mucus, veins were not studied in the simplified model. The stratum corneum typical thickness is 40 μm and was incorporated in both models as boundary condition. The SON was shown with three branches and STN was shown with two branches.

(Synopsys, Mountain View, USA), as shown in Fig. 1a. The skin layer was modeled as stratum corneum (just outside of epidermis layer, as shown in Fig. 1b) and epidermis and dermis layers were considered as a single layer due to their similar conductivity. The exact nerve trajectories could not be identified in the MRI scans. Therefore, realistic SON and STN nerve trajectories were extracted based on data in [13] and [14]. Combined with Cefaly's electrode patch they were modeled from primitive shapes in ScanIP software. To obtain more accurate results, the region of interest was meshed more finely compared with the rest of the model. After arranging volumetric meshes, the 3D volume conductor was exported to a commercial finite element (FE) solver, COMSOL Multiphysics v5.2a (COMSOL, Ltd., Cambridge, UK), to simulate the electric potential field in the model.

B. Simplified Human Head Model Development

It has been shown that the human head can be modeled from geometric shapes (e.g., sphere) to sufficiently accurately model the current flow and electric field in the brain from surface electrodes [15], [16]. Human head tissue layers and surface electrodes (of the same dimension as the Cefaly electrode) were built from concentric spheres in COMSOL. The curvature of the region of interest (forehead) was constructed to follow that of the realistic human head model. To ensure the two models are as similar as possible, the average thicknesses of the realistic segmentation layers were used to construct the layers of the simplified model. The white and gray matters were unified and modeled as brain in this model due to voltage drop decaying considerably after the skull layer.

It is important to have the same nerve trajectories to compare both models. Therefore, the nerve trajectories were generated from the center lines of the realistic nerves using the *'sweep'* function in COMSOL. The stratum corneum layer is comparatively thin and was modeled as '*contact impedance*' during simulations for both human head models.

C. Volume Conduction Simulation

Since in a complicated geometry (such as head volume conductor) the underlying differential equations cannot be solved analytically, the finite element method (FEM) was used to solve for the electrical potential distribution for each medium. The simulations were carried out using COMSOL while observing the quasi-static approximation of Maxwell equations demonstrated by Laplace formulation shown in (1). This has been shown to introduce negligible error in the frequencies involved [17]. The current density on the nerves was calculated from this approximated electric potential for both models based on (2).

$$\nabla.(\sigma\nabla V) = 0 \tag{1}$$

$$J = \sigma\nabla V \tag{2}$$

where, σ, V and J represent each tissue conductivity, electrical potential and current density, respectively. A comparatively large [9] non-conductive (σ = 1e-10 S/m) sphere was defined as external boundary and Dirichlet boundary condition (V = 0) was applied which was considered an approximation of ground at infinity. The conductivity of other layers was set as listed in Table I (low frequency values).

TABLE I. TISSUE CONDUCTIVITIES

Tissue layers	Conductivity (S/m)	Reference
Stratum corneum	2e-4	[18],[19]
Epidermis	0.22	[19], [20]
Dermis	0.22	[19], [20]
Fat	0.025	[18]
Muscle	0.16	[18]
Nerve	1.2	[18]
Eyeball	0.5	[18]
Skull	0.015	[21]
CSF, Sagittal sinuses	1.8	[22]
White matter	0.12	[23]
Gray matter (Brain)	0.1	[18]
Gel	0.1	-

For the numerical approximation in TENS simulation, a geometry adapted tetrahedral FE approach was implemented. To obtain an efficient solution (reduce error) of the TENS FE equation system, the algebraic multigrid preconditioned conjugate gradient and iterative solver method were used. The electrical potential along the nerve trajectories were calculated in each head model to apply as extracellular potential to the nerve cable models.

The segmentation and discretisation time were approximately 8 days and 26 hours, respectively, for the realistic head model. The number of tetrahedral finite elements was about 22 million and the simulation time was 19 minutes for this model. On the other hand, the required time for discretisation time was 3 minutes for the simplified head model. The number of obtained tetrahedral elements was about 2.3 million and the simulation time was 2 minutes.

D. Myelinated Nerve Fiber Model

The nerve fiber excitation was quantified via TES using the McIntyre–Richardson–Grill (MRG) cable model of a myelinated mammalian axon [24]. Fibre distributions and the number of compartments and their geometric positions along the nerve length were designed based on the previous study [9]. The obtained extracellular electrical potential was then exported into Neuron v7.4 [25] to form voltage pulses and apply them to a population of the double layer cable model of mammalian fibers to simulate responses of fibres' [9]. The cable model and a sample set of responses are shown in Fig. 2.

The percentage activation (PA) of fibers was measured based on the fifth current pulse with the Cefaly stimulator parameters (biphasic symmetrical rectangular 250 µs pulses at 60 Hz) [9]. The PAs were firstly calculated for node 0 for 100 fibers and then for node 25. A fiber was considered activated when activation potentials were observed in both. For models in this study the fiber activation onset and safe guard thresholds were considered as 10% and 50% respectively. The realistic and simplified head models are referred to as model A and model B, respectively, in the following results.

III. RESULTS

The PAs of different nerve branches for different stimulus currents for models A and B are shown in Fig. 3. Current

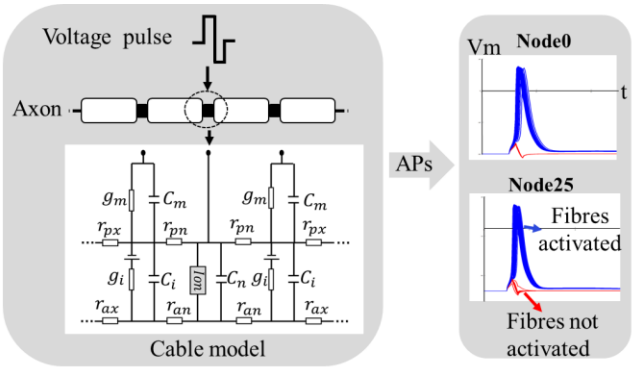

Fig. 2. The cable model and a sample set of responses (action potentials (AP)) are shown. The first and the last point of fiber represented with node0 and node25, accordingly.

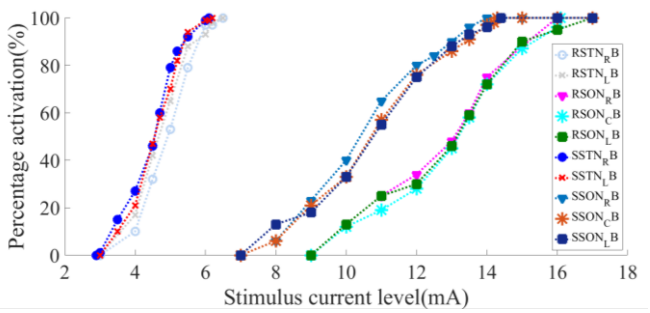

Fig. 3. The PAs of nerve fibers, the PAs versus stimulus current levels are shown for both realistic and simplified head model. The first letter of acronyms show whether the results belong to realistic (R) or simplified (S) model and last two letters are the abbreviation of nerve branches (RB: right branch, CB: center branch, and LB: left branch).

levels of 6.5 mA and 6.1 mA are required to activate all fibers in the right branches of STN for models A and B, respectively. The onset of activation for the right branch of the STN is at about 4 mA for model A and 3.4 mA for model B.

To activate the left branch of the STN for models A and B, the necessary current levels are 6.5 and 6.2 mA, respectively. Model B requires less current to reach the onset of activation on the right branch of the STN compared to model A. All SON branches (right, center and left) are minimally activated at current levels of about 10 mA for model A. However, these branches require lower levels for a minimal activation for model B. To generate APs for all nerve fibers of the right branch of the SON for models A and B, 16 mA and 14 mA are respectively needed. To fully activate the fibers of the center branch of the SON, current levels of 16.1 mA for model A and 14.3 mA for model B are required. All fibers of the left branch of the SON are activated with 17 mA for model A and 14.4 mA for model B. To activate around 50% of the fibers in model A and model B, stimulation current level should be at least 4.7 mA for all branches of the STN. On the other hand, to activate 50% of the fibers in the SON, at least 10.5 mA is needed for model B and 13.5 mA is required for model A.

The current densities on the STN branches are shown in Fig. 4. The current densities on the left branches are nearly identical for both models. However, for the right branches current density values are higher in model A compared to model B.

IV. DISCUSSION

In this study, the impact of volume conductor model complexity on simulated stimulus current levels in hybrid models (coupled volume conductor and nerve fiber model) was investigated. A realistic model and a simplified multi-layer volume conductor model were developed to compare the peripheral nerve excitation and current density for both models.

The simplified trajectories of the SON and STN were considered in [9] while branched trajectories were examined in this paper. It was shown that the nerve branches have an impact on the stimulus current level. The nerve branches which are close to the centerline of the head were activated with a low level of current threshold. To stimulate all nerve

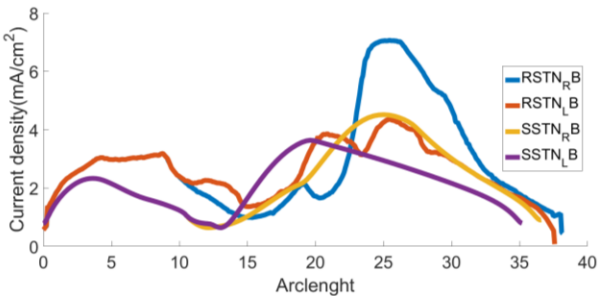

Fig. 4. The current density along the STN arc length are illustrated for both realistic and simplified head model. RSTN and SSTN stand for STN in realistic model and STN in simplified model.

fibers, the difference of the stimulus current threshold levels in models A and B, were about 4% for the left and 6% for right branches of the STN. These differences were 12% for the right, 11% for the center and 15% for the left branches of the SON. This may be associated with current densities near the STN.

Although the detailed head model was constructed by explicitly defining more tissue layers compared with the simplified head model, the simulation results show that there is not a large difference between stimulus current threshold estimates. The reason for high current levels required for the SON activation may be due to the increased locational depth of its trajectory compared with that of the STN.
The reason for high levels of current density in the realistic model may be associated with the finer details and less smooth boundaries in this model compared with the smooth simplified head model.

V. CONCLUSION

Two volume conductors for the human head models (realistic and simplified) and stimulus electrodes were generated to investigate the effect of model complexity on the current density and PAs of the nerve fibers.

This study indicates that a simplified model may be used in future work when assessing the effect of anatomical variations on the efficacy of the target solution and possible ensuing optimizations. A simpler model is more computationally efficient and will take considerably less time to solve. Therefore, a more elaborate matrix of variations of neuroanatomical structures and the neuromodulator may be readily developed to produce a statistically relevant model of the patient group.

REFERENCES

[1] C. Road, "The International Classification of Headache Disorders, 3rd edition (beta version)," Cephalalgia, vol. 33, no. 9, pp. 629–808, 2013.

[2] T. J. Steiner, L. J. Stovner, and G. L. Birbeck, "Migraine: the seventh disabler.," J. Headache Pain, vol. 14, p. 1, Jan. 2013.

[3] C. E. C. L. Arke, L. Ma, I. L. Lan, S. Sondhi, and N. E. J. W. E. L. L. S, "Economic and social impact of migraine," Q J Med, vol. 89, no. March 1994, pp. 77–84, 1996.

[4] H.-C. Diener, A. Charles, P. J. Goadsby, and D. Holle, "New therapeutic approaches for the prevention and treatment of migraine," Lancet Neurol., vol. 14, no. 14, pp. 1010–1022, 2015.

[5] P. Martelletti et al., "Neuromodulation of chronic headaches: position statement from the European Headache Federation.," J. Headache Pain, vol. 14, no. 1, p. 86, Oct. 2013.

[6] D. Magis, S. Sava, T. S. d'Elia, R. Baschi, and J. Schoenen, "Safety and patients' satisfaction of transcutaneous supraorbital neurostimulation (tSNS) with the Cefaly® device in headache treatment: a survey of 2,313 headache sufferers in the general population.," J. Headache Pain, vol. 14, p. 95, 2013.

[7] K. D. Ostilio and D. Magis, "Invasive and Non-invasive Electrical Pericranial Nerve Stimulation for the Treatment of Chronic Primary Headaches," Curr. Pain Headache Rep., vol. 20, no. 11, 2016.

[8] A. J. Sinclair, A. Sturrock, B. Davies, and M. Matharu, "Headache management: pharmacological approaches," Pract. Neurol., vol. 15, no. 6, pp. 411–423, 2015.

[9] E. Salkim, A. N. Shiraz, A. Demosthenous, "Effect of Nerve Variations on the Stimulus Current Level in a Wearable Neuromodulator for Migraine : A Modeling Study," 2017, pp. 239–242.

[10] S. Raspopovic, F. M. Petrini, M. Zelechowski, and G. Valle, "Framework for the Development of Neuroprostheses: From Basic Understanding by Sciatic and Median Nerves Models to Bionic Legs and Hands," Proc. IEEE, vol. 105, no. 1, 2016.

[11] M. Capogrosso et al., "A Computational Model for Epidural Electrical Stimulation of Spinal Sensorimotor Circuits," J. Neurosci., vol. 33, no. 49, pp. 19326–19340, 2013.

[12] M. I. Iacono et al., "MIDA: A Multimodal Imaging-Based Detailed Anatomical Model of the Human Head and Neck," PLoS One, vol. 10, no. 4, p. e0124126, Apr. 2015.

[13] K. N. Christensen, N. Lachman, W. Pawlina, and C. L. Baum, "Cutaneous Depth of the Supraorbital Nerve," Dermatologic Surg., vol. 40, no. 12, pp. 1342–1348, 2014.

[14] K.-J. Shin, H. J. Shin, S.-H. Lee, W.-C. Song, K.-S. Koh, and Y.-C. Gil, "Emerging Points of the Supraorbital and Supratrochlear Nerves in the Supraorbital Margin With Reference to the Lacrimal Caruncle," Dermatologic Surg., vol. 42, no. 8, pp. 992–998, 2016.

[15] S. Rush and D. A. Driscoll, "Current distribution in the brain from surface electrodes.," Anesth. Analg., vol. 47, no. 6, pp. 717–23, 1968.

[16] A. Datta, M. Elwassif, F. Battaglia, and M. Bikson, "Transcranial current stimulation focality using disc and ring electrode configurations: FEM analysis," J. Neural Eng., vol. 5, no. 2, pp. 163–174, 2008.

[17] R. Plonsey and D. B. Heppner, "Considerations of quasi-stationarity in electrophysiological systems," Bull. Math. Biophys., vol. 29, no. 4, pp. 657–664, 1967.

[18] C. Gabriel et al., "The dielectric properties of biological tissues: I. Literature survey," Phys. Med. Biol., vol. 41, no. 11, pp. 2231–2249, Nov. 1996.

[19] T. Yamamoto and Y. Yamamoto, "Electrical properties of the epidermal stratum corneum," Med. Biol. Eng., vol. 14, no. 2, pp. 151–158, 1976.

[20] V. De Santis, X. L. Chen, I. Laakso, and A. Hirata, "An equivalent skin conductivity model for low-frequency magnetic field dosimetry," Biomed. Phys. Eng. Express, vol. 1, no. 1, p. 15201, 2015.

[21] T. F. Oostendorp, J. Delbeke, and D. F. Stegeman, "The conductivity of the human skull: Results of in vivo and in vitro measurements," IEEE Trans. Biomed. Eng., vol. 47, no. 11, pp. 1487–1492, Nov. 2000.

[22] S. B. Baumann, D. R. Wozny, S. K. Kelly, and F. M. Meno, "The electrical conductivity of human cerebrospinal fluid at body temperature," IEEE Trans. Biomed. Eng., vol. 44, no. 3, pp. 220–225, Mar. 1997.

[23] R. N. Holdefer, R. Sadleir, and M. J. Russell, "Predicted current densities in the brain during transcranial electrical stimulation.," Clin. Neurophysiol., vol. 117, no. 6, pp. 1388–97, Jun. 2006.

[24] C. C. McIntyre, A. G. Richardson, and W. M. Grill, "Modeling the excitability of mammalian nerve fibers: influence of afterpotentials on the recovery cycle.," J. Neurophysiol., vol. 87, no. 2, pp. 995–1006, 2002.

[25] M. L. Hines and N. T. Carnevale, "The NEURON simulation environment.," Neural Comput., vol. 9, no. 6, pp. 1179–1209, Aug. 1997